Design, Analyses, and Model Tests of an Aeroelastically Tailored Lifting Surface

W.A. Rogers* and W.W. Braymen*
General Dynamics, Fort Worth Division, Fort Worth, Texas
and
M.H. Shirk†
AFWAL, Flight Dynamics Laboratory, Wright-Patterson Air Force Base, Ohio

Aeroelastic tailoring provides a measure of control over the interaction of aerodynamic loading and structural response during the design of composite lifting surfaces. A recent investigation involving the design, fabrication, and test of an aeroelastically tailored fighter wing was conducted to provide data for validating the design methodology. Three sets of composite wings with different design objectives were tested in addition to a set of rigid steel wings. The static aeroelastic tests featured the measurement of model forces, pressure distributions, and deflected shapes in the transonic regime. Test results are compared with analytical predictions and show significant aeroelastic benefits.

Introduction and Background

THE concept of structurally tailoring an advanced composite wing box for beneficial static deformation under airload was first proposed by M.E. Waddoups and published in an Air Force Technical Report[1] a decade ago. The concept is known as aeroelastic tailoring because the aeroelastic response of the lifting surface is designed by tailoring the stiffness distribution of the structure. It is well known that ply orientations and thickness distributions may be easily varied in the composite laminate to design the material characteristics needed for the specific application. Aeroelastic tailoring is a logical extension of the application of advanced composites to aircraft structure in view of the design freedom offered by this material, a freedom which does not exist in conventional metallic structure.

The design for a desired static aeroelastic response was initially an iterative process performed by a structural engineer trying to satisfy a requirement for twist and camber established by an aerodynamicist. Laminate orientation and thickness distribution of each orientation were arbitrarily selected and an analysis performed for a given airload and inertia load distribution. A number of laminates were defined and analyses performed until a data base had been generated which could be used for guiding the selection of a subsequent laminate. When a laminate was defined that satisfied twist and camber requirements, the design was checked for strength and flutter. Obviously this process was very time consuming. The development of structural optimization methods in the late 1960s led to an Air Force contract requirement for a "pilot" method for the design of a composite lifting surface for which strength and flutter requirements could be simultaneously satisfied by taking advantage of the design latitude available with advanced composites. Under this contract General Dynamics developed the Wing Aeroelastic Synthesis Procedure[2,3] (generally referred to as TSO).

Applications of the aeroelastic tailoring concept were made to a few wing configurations by the AFFDL both on an in-house basis[4,5] and under contract. General Dynamics performed parameter studies and applied the aeroelastic tailoring technology to a fighter configuration (for reduced maneuver drag) and a high-aspect-ratio variable-sweep bomber configuration (for range improvement).[6,7] Grumman applied aeroelastic tailoring to an advanced design composite aircraft and showed beneficial results for the vertical tail (for improved effectiveness), but very little benefit for the wing of this low-load-factor supersonic airplane.[8]

NASA initiated the third phase of their highly maneuvering aircraft technology (HiMAT) program in 1975 with a contract award to Rockwell International to design and fabricate a remotely piloted research vehicle (RPRV) incorporating technologies applicable to an advanced highly maneuverable fighter configuration. Aeroelastic tailoring was one of the technologies selected which provides reduced drag in maneuver and results in a higher-load-factor capability.[9] Application studies have also been performed by Boeing[10,11] and McDonnell.[12]

In 1978 a program was initiated to validate the aeroelastic tailoring design methods. This validation was to be accomplished through the correlation of the design procedures with static aeroelastic and flutter model wind tunnel testing. This article describes the validation program and presents results for the static aeroelastic portion of the program. The accomplishments in this program illustrate that aerodynamic benefits can be obtained by taking advantage (through design) of aeroelastic response. A design approach is available through which these advantages can be realized.

Design Objectives and Methods

The objectives of the validation program were to obtain wind tunnel data for tailored wing designs and demonstrate the range of beneficial aeroelastic response attainable through the choice of design objective for a given planform configuration. Reference 13 provides a complete description of this effort.

Configuration Selection

The wing/body-of-revolution/strake configuration illustrated in Fig. 1 was selected for the study. The wing planform was the outgrowth of an independent research and development program concerned with providing good transonic maneuverability without sacrificing supersonic

Presented as Paper 81-1673 at the AIAA Aircraft Systems and Technology Conference, Dayton, Ohio, Aug. 11-13, 1981; submitted Aug. 20, 1981; revision received June 28, 1982.

*Engineering Specialist. Member AIAA.
†Principal Scientist, Analysis and Optimization Branch, Structures and Dynamics Division. Member AIAA.

performance.[14] It was also very similar to a fighter wing that showed aeroelastic tailoring potential during a previous contract study.[7] Inclusion of the strake provided further representation of current advanced fighters. In addition, the configuration was one that had been wind tunnel tested previously with a blended fuselage, providing a data base for comparison with the body-of-revolution research model.

Three sets of aeroelastic wings were designed in addition to a set of "rigid" steel wings. The aeroelastic wings were representative of different tailoring objectives. The aerodynamic objective sought with the first aeroelastically tailored wing was reduced drag at transonic maneuver conditions through achievement of aeroelastic camber and negative twist (washout). The aerodynamic benefit of the second tailored wing was to demonstrate increased lift-curve slope through positive twist (washin) and camber. Such a design is directly applicable to vertical-tail surfaces, where loss of effectiveness due to aeroelastic effects often results with conventional designs. The washout and washin wing designs provided two significantly different concepts for methods evaluation, while illustrating the wide range of design control available with composites. The third aeroelastic wing, referred to as nontailored, was designed to simulate a balanced composite wing laminate where equal amounts of crossplies are used. Comparison of the test data from the nontailored wing with that from the tailored wings provided a measure of the benefits resulting from aeroelastic tailoring. The steel wing established a conventional model testing data base from which to measure the aeroelastic increments.

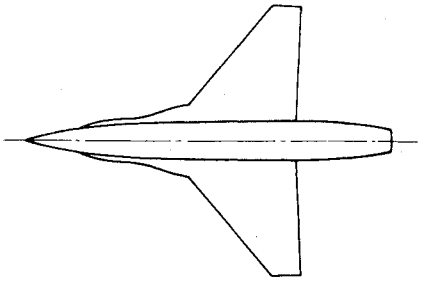

• WING	FULL SCALE
AREA	338.29 Ft^2
SPAN	399.726 In.
THEO ROOT CHORD	200.738 In.
MAC, $\bar{c}$	138.882 In.
ASPECT RATIO	3.28
TAPER RATIO	0.2142
SWEEP	40.0°
AIRFOIL	NACA 64A004 @ Tip NACA 64A003.5 @ Root
INCIDENCE	0°
TWIST	0°
• FUSELAGE	
OVERALL LENGTH	547.000 In.
MAX BODY DIA	55.400 In.

Fig. 1 Selected wing/body/strake configuration.

Full-Scale Design

The structural geometry of the full-scale designs is shown in Fig. 2. A design condition with a Mach number of 0.9, an altitude of 10,000 ft, and a load factor of 9g was used. All designs were constrained to have minimum values of flutter speeds and roll effectiveness commensurate with an aluminum baseline design.

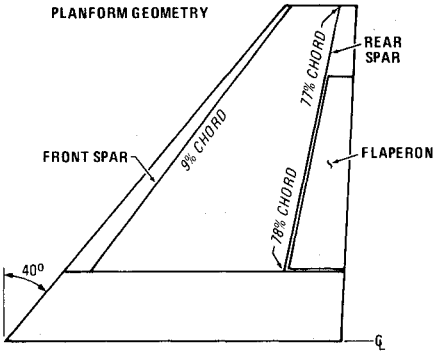

Fig. 2 Structural geometry.

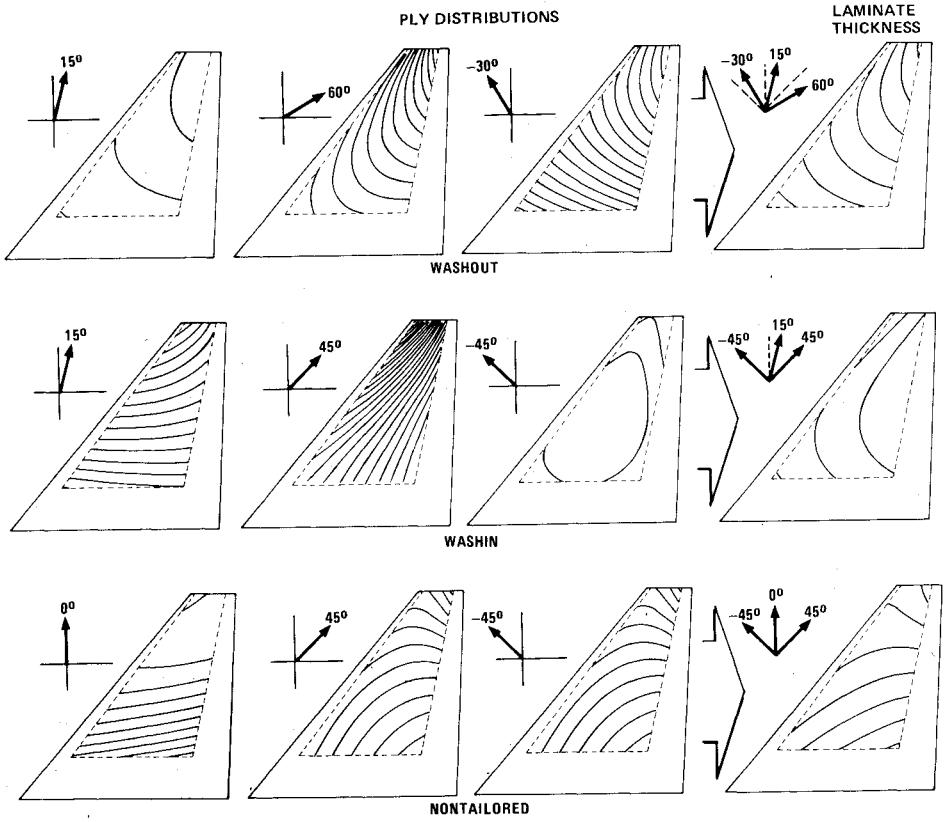

Fig. 3 Ply distributions for full-scale designs.

Numerous full-scale designs were evaluated, and three different configurations were selected to provide a wide range of aeroelastic twist. The washout design was the result of a TSO objective function using a minimum structural weight and maximum negative twist near the wing tip, while the washin wing resulted from an objective function of minimum structural weight and maximum positive twist. The nontailored wing, representative of a more conservative design approach, was the result of having only minimum weight as the objective function. The resulting ply orientations and thickness contours are shown in Figure 3. The full-scale washout wing is unusual in that unidirectional glass fibers are used for the spanwise plies, while all other ply orientations consist of unidirectional graphite.

Model Design

The 1/9-scale model consisted of a body of revolution with removable forebody strakes and aeroelastic wing panels and was supported in the tunnel by a sting. The wings were pinned to a centerbody adapter, as shown in Fig. 4, to permit configuration changes.

The aeroelastic models were designed for testing in the Arnold Engineering Development Center (AEDC) PWT-16T wind tunnel. A dynamic pressure of 750 psf was chosen (slightly within the tunnel capability) to represent the full-scale flight condition of 1.2 Mach number, 10,000 ft altitude, and 1467 psf dynamic pressure. The resulting scale factor for dynamic pressure was $750/1467 = 0.511$.

The design of the model wing laminates required preserving the scaled flexibility characteristics of the full-scale wings while satisfying flutter requirements and demonstrating a proof-loading to twice the maximum aerodynamic load expected in the wind tunnel. The strength criterion required the model wings to be stronger than their full-scale counterparts. Previous experience with a high-strength aeroelastic model[1,15] suggested the use of a hybrid laminate of unidirectional glass-epoxy and graphite-epoxy to provide sufficient strength without excessive stiffness. Glass-epoxy and graphite-epoxy tape with cured ply thicknesses of 0.0023 and 0.0018 in., respectively, were used to preserve the stiffness distribution of the full-scale wings.

The TSO program was used in the model design phase to determine the thickness distributions of the laminates.

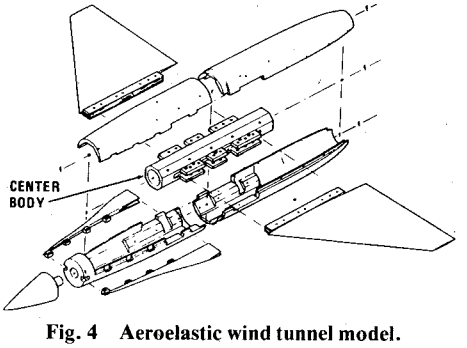

Fig. 4 Aeroelastic wind tunnel model.

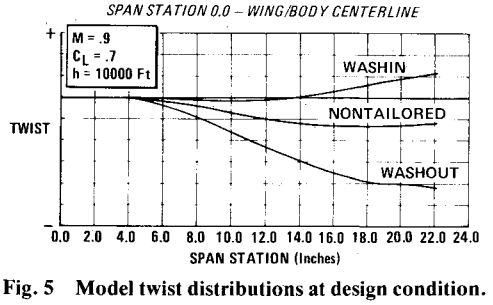

Fig. 5 Model twist distributions at design condition.

Comparison of scaled deflections of the model with the desired full-scale deflection is the accepted method for measuring the success of a flexible model. For greater visibility the spanwise distribution of twist and camber under aerodynamic load were compared between model and full-scale. The wing twist was defined as the difference between the front and rear spar deflections divided by the local chord length. Twist and camber distributions of the models at the design condition are shown in Figs. 5 and 6. The camber was defined by using the deflection at a location midway between the front and rear spar.

Instrumentation

Several types of instrumentation were considered essential to provide the information necessary to evaluate the design methods. Since the aerodynamic and structural methods are interdependent in the tailoring process, it was necessary to include sufficient instrumentation to allow independent evaluation of the aerodynamic as well as the structural simulation used in TSO. As a result, instrumentation was included in the design of the model as described below.

1) An internal six-component balance served to measure complete model forces and moments.

2) Ninety-eight static pressure orifices were located on the upper and lower surfaces of the aeroelastic wings to measure the chordwise and spanwise load distribution. Upper-surface pressure distributions were measured on the right wing panel, and lower-surface pressures were measured on the left panel. Pressures were recorded with 48-port scani-valves located in the nose of the model. Although complete pressure distributions were obtained on the aeroelastic wings, only one row of five orifices was located along the upper-surface leading edge of the rigid wing to provide comparison of leading-edge flow separation characteristics with corresponding results from the aeroelastic wings.

3) Photographic targets were installed on the wings and fuselage to allow determination of wing deflections through the use of photogrammetry.[16] The technique involves obtaining a simultaneous pair of photographs of the model from two viewpoints above using stroboscopic lighting and, thus, providing complete instantaneous documentation of the model deflection. The technique was used during both the laboratory tests and wind tunnel tests to record the wing aeroelastic shape. Optical targets consisting of a white dot on a contrasting dark background were positioned on the wing. Reference targets were also placed on the fuselage (for the wind tunnel tests) or on an alternate rigid structure (for the laboratory tests). Forty-nine wing targets were positioned to provide definition of aeroelastic twist and camber. Reference coordinates of these targets were obtained from pretest model inspections and from analysis of air-off photographs obtained during the wind tunnel tests. Data reduction of each stereo pair provides for a solution of a system of equations that yields the location of each target in three dimensions.

4) Foil strain gages located on the upper and lower surfaces of the left wing panel and on the centerbody tabs provided steady-state and dynamic measurements of bending moment. Dynamic measurements of bending moment were also ob-

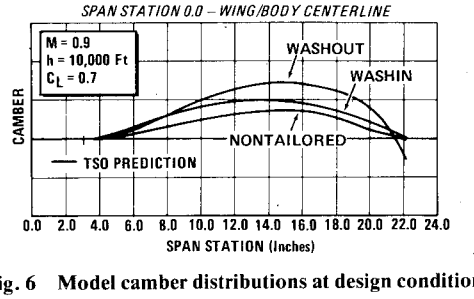

Fig. 6 Model camber distributions at design condition.

tained from a semiconductor gage located on the upper left wing panel.

Model Fabrication

The fuselage body components and strakes were machined from 7075 aluminum while the centerbody and rigid wings were machined from 4340 steel. The aeroelastic wings were fabricated from glass-graphite-epoxy laminates and Nomex® core. Left-hand and right-hand steel female tools were fabricated for the lay-up and cure of the laminates. The steel molds provided close control of the wing external geometry. Mylar templates for each ply assured accurate placement and orientation of the plies during stacking in the mold. The skin laminates were cured at elevated temperature and pressure in a cavity press.

The cured laminates were returned to the molds for the bonding of Nomex® honeycomb core at room temperature. Potting compound was added to the leading and trailing edges, and the cores were milled to the wing chord plane. Additional milling of the core in selected areas provided for installation of the steel pressure tubes, as shown in Fig. 7. The upper and lower halves of the wing were bonded together with sheet adhesive. The edges of the wing were wrapped with a single ply of fiberglass cloth. Steel contour blocks were fitted to the upper and lower contour surfaces to permit attachment to the model centerbody.

Laboratory Tests

Each aeroelastic wing panel was proof-loaded to 1000 lb. The distributed load was applied at 12 locations on the wing using a whiffle-tree fixture attached to a hydraulic ram, as shown in Fig. 8. Strain gage readings were recorded, a visual indication of the trailing-edge deflection was observed at the wing tip, and the aeroelastic shape was recorded using photogrammetry.

Ground vibration tests were also conducted on each set of aeroelastic wings. The complete model, including centerbody, was softly supported from springs and tested as a free-free model. Laboratory tests were also conducted at AEDC to determine whether the model's vibration characteristics were adversely affected on the wind tunnel test sting and balance. The fundamental antisymmetric bending mode of each model was the only mode that varied significantly between spring-supported and sting-supported tests. The flutter analyses at Mach 0.9 using measured modes indicated large flutter margins for all models.

Wind Tunnel Test

The wind tunnel test was conducted in the AEDC PWT-16T wind tunnel from September 28 to October 5, 1979. For each wing, data were obtained at Mach numbers from 0.6 to 1.2 at dynamic pressures simulating altitudes from sea level to 30,000 ft. Data were obtained at angles of attack from -10 to $+28$ deg, with limits dependent on Mach number and dynamic pressure. Directional stability data were obtained from -10 to $+10$ deg of sideslip for selected Mach number/altitude conditions.

A unique feature of the test was the simultaneous acquisition of all data—force, pressure, aeroelastic shape documentation, and steady-state and dynamic bending moment, as well as motion pictures. Oil-flow photographs were also obtained at selected conditions.

Early in the test, the rigid wing was utilized to establish if changes in grit size or variations in Reynolds number significantly affected the aerodynamic characteristics, particularly drag due to lift. Neither was found to be a problem, providing confirmation that aeroelastic effects could be measured on these thin wings without significant interplay of Reynolds number effects as dynamic pressure was varied.

Summary of Test Results

The washout wing objective of demonstrating reduced transonic drag due to lift was achieved, as shown in Fig. 9, which compares wind tunnel test drag data for each of the four wings at the design condition of Mach 0.9 and an altitude of 10,000 ft. Comparison with the rigid wing results shows that the drag benefit produced by aeroelastic twist and camber increases with increasing lift up to the 9g design lift coefficient of 0.7, above which the aeroelastic effects begin to decrease from the onset of upper-surface flow separation. At 0.7 lift coefficient, a 23% reduction in drag due to lift was measured. The nontailored wing also showed significant reduction in drag up to moderate values of lift, though most of the effect was lost as a result of flow separation at the 0.7 design lift coefficient. The washin wing also shows reduced drag compared to the rigid wing due to aeroelastic camber.

Lift-curve test results corresponding to the drag results are presented for each of the wings in Fig. 10. These data confirm that the washin wing achieved its objective of demonstrating increased lift-curve slope through aeroelastic tailoring. In the

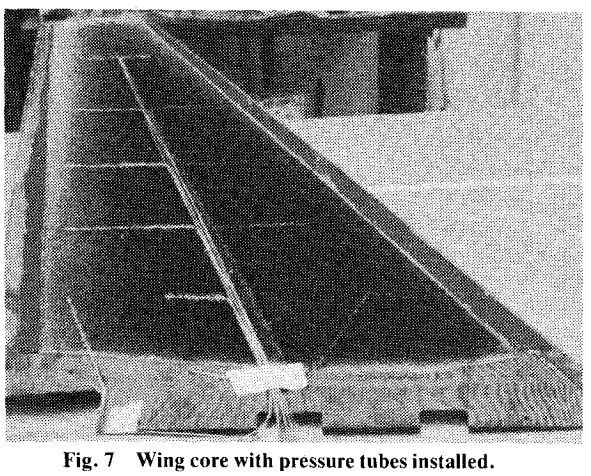

Fig. 7 Wing core with pressure tubes installed.

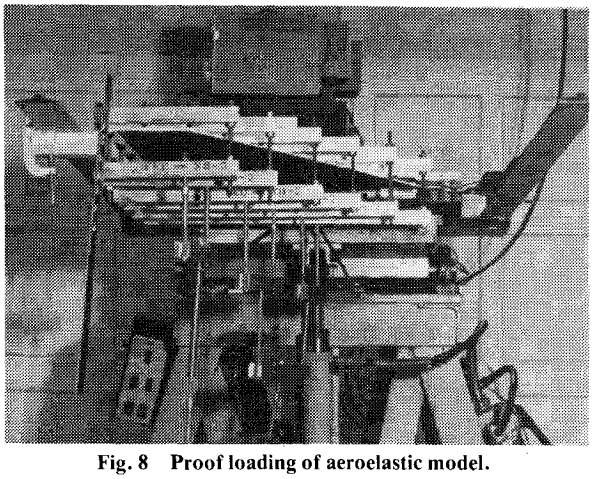

Fig. 8 Proof loading of aeroelastic model.

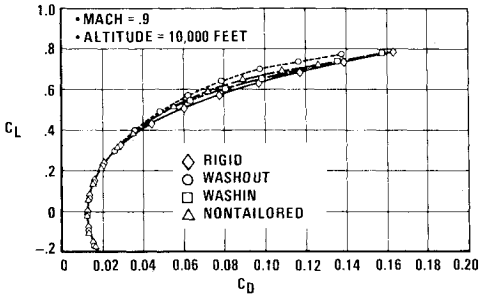

Fig. 9 Drag characteristics at design condition.

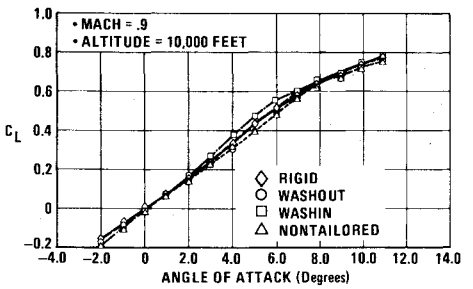

Fig. 10 Lift characteristics at design condition.

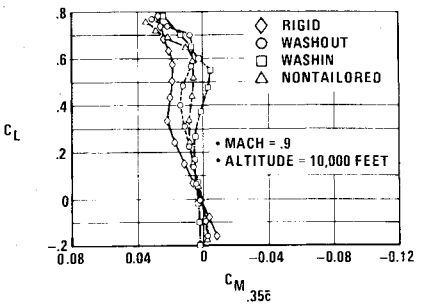

Fig. 11 Pitching moment characteristics at design condition.

angle-of-attack range between −2 and +4 deg, a 16% increase in lift-curve slope was achieved compared to the rigid wing.

Pitching moment results at the Mach 0.9 design condition are shown in Fig. 11 for the four wings. The washout wing shows an aft aerodynamic center (a.c.) shift compared to the rigid wing and achieves the highest lift coefficient before an unstable break occurs at the design lift coefficient. Additional tests with a horizontal tail would be needed to determine if the unstable break is a significant problem.

Additional insight into the flow characteristics present on the washout and washin wings at the design condition is revealed by oil-flow photographs, which are presented in Fig. 12. Both the left and right washout wings were painted with oil, but only the left washin wing was painted. The washin wing shows a large region of separated flow from the leading edge outboard of the midspan. The flow pattern over the washout wing is much better behaved with evidence of separation only near the tip. The classic forward and rear shocks which coalesce near the tip are clearly evident on the right wing. The pressure difference across the shock combined with the component of spanwise flow results in a complex helical pattern at the tip that is more developed on the right wing than on the left. This slight difference in the left and right wings is particularly interesting since the break in the pitching moment curve shown in Fig. 11 occurs at the same point, which is indicative of a transition in flow condition.

The oil-flow results are confirmed by the pressure distributions shown in Fig. 13. (As mentioned earlier, only one spanwise row of orifices was present on the rigid wing.) These comparisons clearly show that the washout wing is accomplishing its objective of delaying upper-surface separation. Flow at the leading edge is attached at all span stations, and trailing-edge separation is evident only at the most outboard station shown. The other three wings show indications of both leading- and trailing-edge separation at $\eta = 0.60$, which becomes progressively worse toward the wing tip.

Stereo photographic negatives were analyzed to provide aeroelastic deflections. Each negative typically contained 113 targets on the model. Fifteen of the targets were located on the model fuselage and served as the control points for the photogrammetric regression analysis. The lateral deflection of the wing panels (in a direction normal to the wing-chord plane) for the design condition of Mach 0.9 and an altitude of 10,000 ft is shown in Fig. 14 for the washout model. The deflections for both left and right panels are presented, indicating negative twist at the tip.

Test-to-Theory Comparisons

The test data from each of the wings were used to establish overall test-to-theory comparisons as well as comparisons aimed specifically at evaluation of the aerodynamic and structural design methods. Calculated aerodynamic forces, moments, and pressures were determined using the following three approaches:

1) Carmichael[17] linear theory predictions with aeroelastic characteristics based on the TSO structural simulation. This

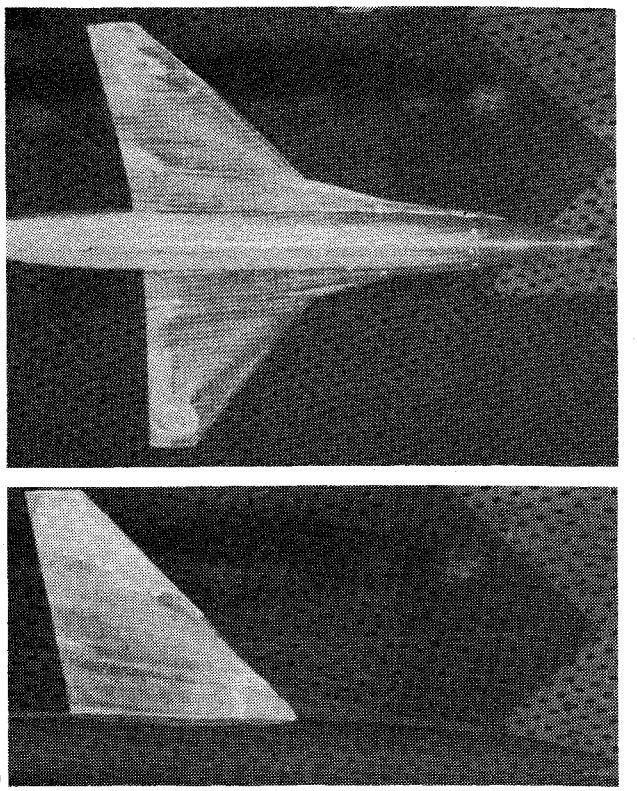

Fig. 12 Comparison of washout and washin wing oil-flow photographs at design condition: Mach = 0.90, altitude = 10,000 ft, $C_L = 0.70$, $\alpha = 8.9$ deg, a) washout wing, b) washin wing.

provided an evaluation of the overall TSO aerodynamic/structural representation.

2) Carmichael linear theory calculations based on aeroelastic geometry as determined from in-tunnel photogrammetry results.

3) Bailey-Ballhaus[18] transonic finite-difference nonconservative calculations based on aeroelastic geometry as determined from the photogrammetry results used in approach 2 above.

Since approaches 2 and 3 do not depend on simulation of the structure, comparison of the two provide an assessment of linear theory as used in TSO relative to a nonlinear transonic code. However, it is noted that, while the Carmichael simulations included the fuselage and strake, the Bailey-Ballhaus analyses represented only the wing. This choice was based on test-to-theory correlations made in an earlier study.[19] Results there showed that the highly swept strake produced a mathematically unacceptable skewed mesh arrangement.

Test-to-theory comparisons based on the three approaches enumerated above are presented here for the washout wing at the design condition of Mach 0.9 and an altitude of 10,000 ft. Figure 15 shows the lift curve comparisons as well as the aeroelastic shift in angle of attack at constant lift coefficient

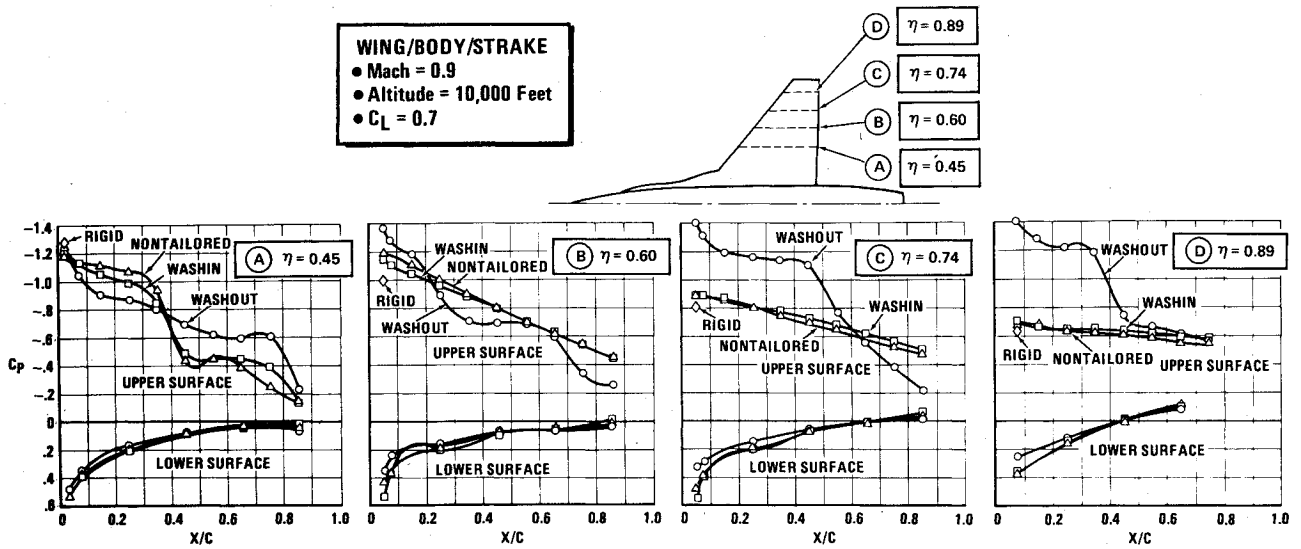

Fig. 13 Comparison of pressure distributions at design condition.

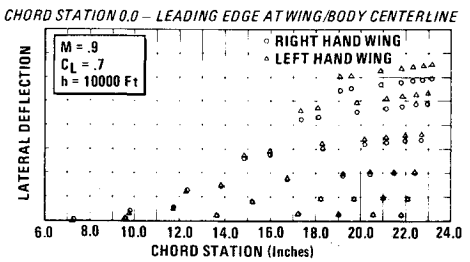

Fig. 14 Model deflections for washout wing in wind tunnel.

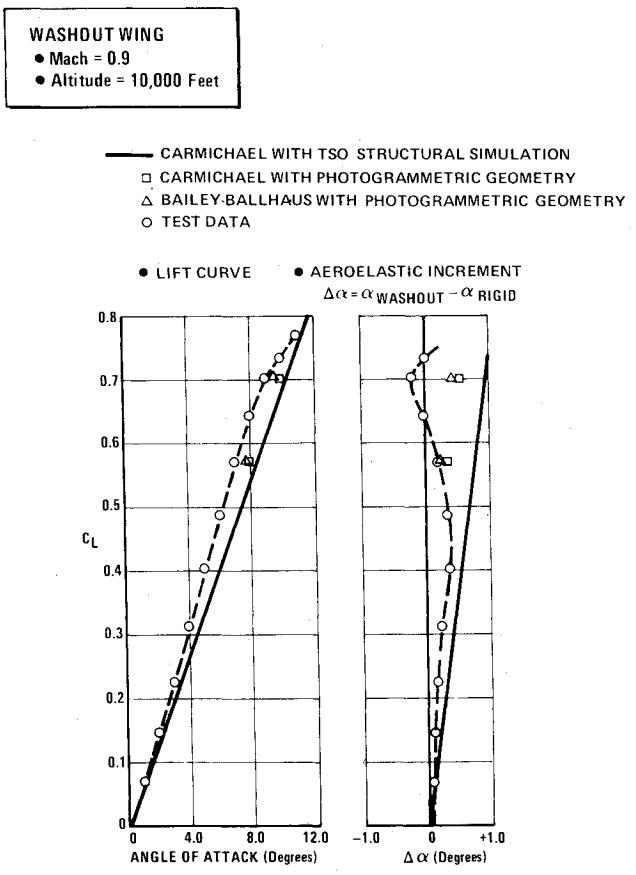

Fig. 15 Test-to-theory correlations of washout wing lift characteristics.

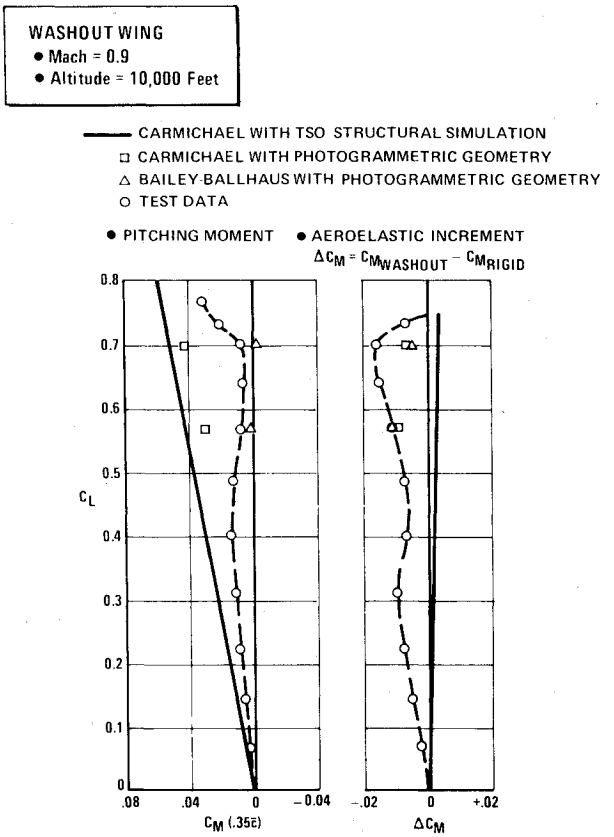

Fig. 16 Test-to-theory correlations of washout wing pitching moment characteristics.

between the washout and rigid wings. Note that the TSO predictions are shown for the entire C_L range, but the calculations dependent on having in-tunnel aeroelastic geometry are shown only at lift coefficients of 0.57 and 0.70, which correspond to points where photogrammetric data were obtained. These results show each of the methods to underpredict the lift, due in part to the inability of any of the methods to account for the vortex lift generated by the strake. (As stated above, the Bailey-Ballhaus representation did not include the strake.) Improvement is obtained when photogrammetric data are used, with the Bailey-Ballhaus results being slightly better. These same trends are exhibited in the aeroelastic increments, shown also in Fig. 15.

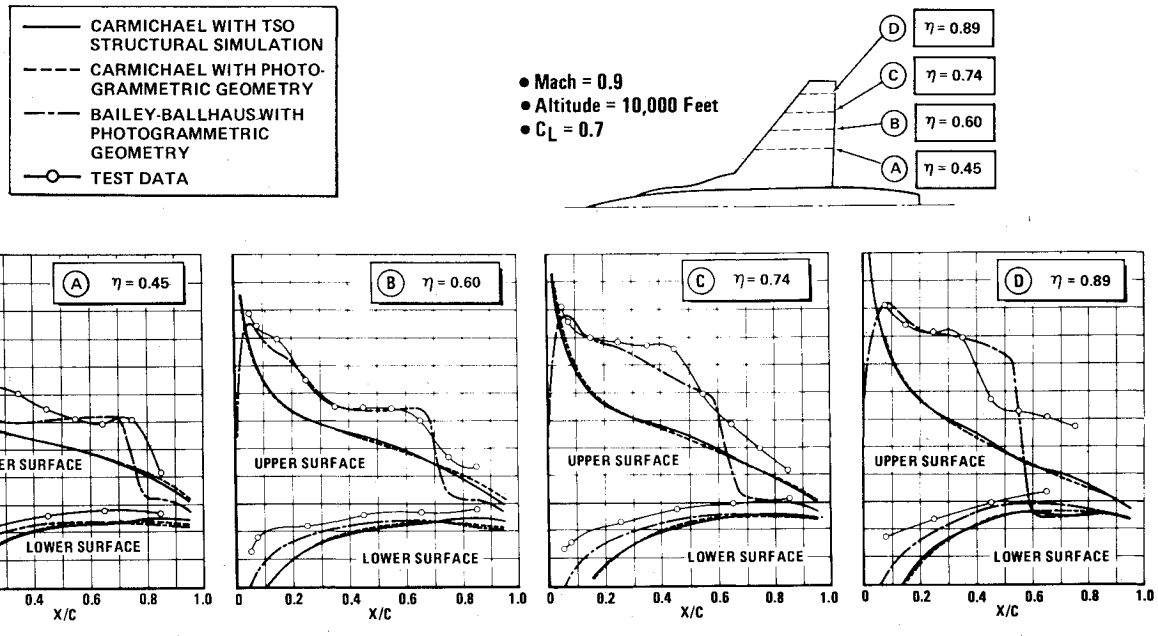

Fig. 17 Test-to-theory correlations of washout wing pressure distributions at design condition.

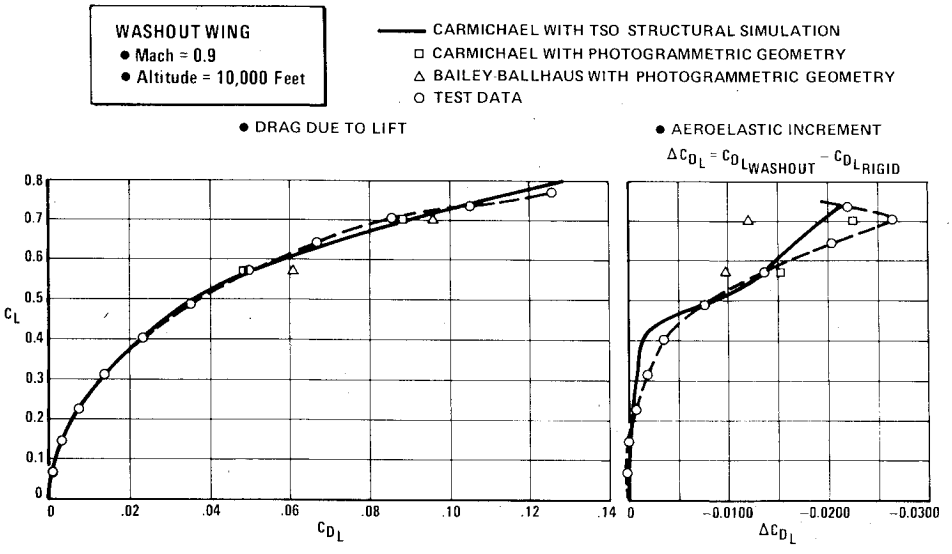

Fig. 18 Test-to-theory correlations of washout wing drag-due-to-lift characteristics.

Pitching moment comparisons corresponding to the lift results are presented in Fig. 16. TSO predicts an a.c. somewhat ahead of the test data. As in the case of lift, use of photogrammetry data improves the correlation. The Bailey-Ballhaus results are very good, owing to its ability to include shock effects, which shift the a.c. aft. While there is considerable difference in calculated moment between Bailey-Ballhaus and Carmichael (using photogrammetric data), the calculated aeroelastic increments agree closely.

Pressure distributions corresponding to the lift and moment results are compared in Fig. 17 at the design lift coefficient of 0.7. The predicted TSO results and Carmichael calculations (with test geometry) show only slight differences between them. Since both are based on linear theory, upper surface shock effects are not predicted. The Bailey-Ballhaus results clearly provide the best correlation of upper- and lower-surface pressures because of the method's ability to account for mixed flow conditions. Leading-edge pressures correlate very well and the general characteristics of the flow are modeled. However, the shock strength is overpredicted, resulting in a loading aft of the shock that is too low (actually negative at the most outboard station). Furthermore, the disagreement between test and theory at the outermost station is magnified as a result of trailing-edge separation. The predicted shock location is slightly forward of the test data at $\eta = 0.45$, but the separated flow near the tip causes the experimental shock to move forward, resulting in a predicted shock that is too far aft.

Comparisons of drag due to lift are presented in Fig. 18. The predicted TSO results incorporate empirical techniques to account for partial leading-edge suction below the polar break lift coefficient and to determine an estimate of the polar break point.[7] Above the polar break, the linear theory zero-suction polar shape is used directly. The Bailey-Ballhaus calculations do not correlate as well as do the linear theory approaches. However, it is noted that the Bailey-Ballhaus method contains no empirical adjustment. This could be an important consideration if test data on a similar configuration were not available.

Figure 18 also shows comparisons of the aeroelastic drag-due-to-lift increment between the washout and rigid wings. The drag benefit attributed to aeroelastic tailoring is generally larger than predicted. The use of photogrammetric data

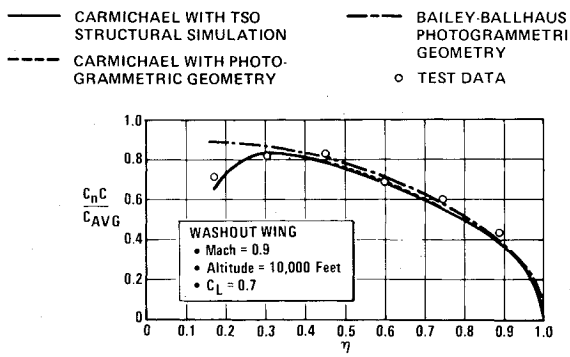

Fig. 19 Test-to-theory correlations of washout wing spanwise load distribution at design condition.

improves the linear theory results, but the Bailey-Ballhaus increments are significantly underpredicted.

Span load distributions at $C_L = 0.70$ are compared in Fig. 19. The drop in loading for the most inboard span station is caused by the fact that the strake was located ahead of the wing and the strake loads were not included. Since the linear theory simulations modeled the strake, the decrease in wing loads also occurs; however, the Bailey-Ballhaus model did not include the strake and consequently does not show the decreased loading. The overall correlations with test data are quite good for all three methods.

Conclusions

The scope of this paper has been limited to a presentation of a summary of the overall investigation. However, several conclusions can be drawn from the highlights presented here. The design objectives were met for each of the tailored wings. Specifically, the washout wing produced significant reduction in transonic drag due to lift compared to the nontailored and rigid wings. The washin wing also accomplished its objective of providing increased lift-curve slope due to aeroelastic tailoring. These results demonstrate that aeroelastic tailoring is an additional tool for the designer.

The Bailey-Ballhaus results showed improved correlation of aerodynamic loads, but there are problems associated with its use in a preliminary design procedure such as TSO. Linear theory is attractive owing to the large number of design iterations required in TSO, while the Bailey-Ballhaus procedure is nonlinear and requires of itself a large number of iterations to establish a solution. Also, simulation of specific geometries such as a strake produces problems. Therefore the future for improving the TSO aerodynamic simulation appears to lie in the development of quasilinearized transonic codes.

The wind tunnel test provided a comprehensive set of data to evaluate the design methods. The large data base should be useful in future methods development. Photogrammetry was a valuable and necessary tool for establishing accurate aeroelastic geometry in the wind tunnel.

Acknowledgment

This research was sponsored by the Air Force Wright Aeronautical Laboratories, Flight Dynamics Laboratory, Wright-Patterson AFB, Ohio.

References

[1] Waddoups, M.E. et al., "Composite Wing for Transonic Improvement," AFFDL-TR-71-24, Vols. I and II, Air Force Flight Dynamics Laboratory, Wright-Patterson Air Force Base, Ohio, Nov. 1971.

[2] McCullers, L.A. and Lynch, R.W., "Composite Wing Design for Aeroelastic Tailoring Requirements," Paper presented at the Air Force Conference on Fibrous Composites in Flight Vehicle Design, Dayton, Ohio, Sept. 26-28, 1972.

[3] McCullers, L.A. and Lynch, R.W., "Dynamic Characteristics of Advanced Filamentary Composite Structures," AFFDL-TR-73-111, Vols. I-III, Air Force Flight Dynamics Laboratory, Wright-Patterson Air Force Base, Ohio, Sept. 1974.

[4] Shirk, M.H. and Griffin, K.E., "The Role of Aeroelasticity in Aircraft Design with Advanced Filamentary Composite Materials," Paper presented at the Second Conference on Fibrous Composites in Flight Vehicle Design, Dayton, Ohio, May 1974.

[5] Griffin, K.E., "An Aeroelastic Tailoring Study of a High Aspect Ratio Wing," Paper presented at the Third Conference on Fibrous Composites in Flight Vehicle Design, Williamsburg, Va., Nov. 4-6, 1975.

[6] Lynch, R.W. and Rogers, W.A., "Aeroelastic Tailoring of Composite Materials to Improve Performance," Paper presented at the AIAA/ASME/SAE 17th Structures, Structural Dynamics, and Materials Conference, King of Prussia, Pa., May 5-7, 1976.

[7] Lynch, R.W., Rogers, W.A., and Braymen, W.W., "Aeroelastic Tailoring of Advanced Composite Structures for Military Aircraft," AFFDL-TR-76-100, Vols. I-III, Air Force Flight Dynamics Laboratory, Wright-Patterson Air Force Base, Ohio, Feb. 1978.

[8] Austin, E., Hadcock, R., Hutchings, R., Sharp, D., Tang, S., and Waters, C., "Aeroelastic Tailoring of Advanced Composite Lifting Surfaces in Preliminary Design," Paper presented at the AIAA/ASME/SAE 17th Structures, Structural Dynamics, and Materials Conference, King of Prussia, Pa., May 5-7, 1976.

[9] Lockenour, J.L. and Layton, G.P., "RPRV Research Focus on HiMAT" *Astronautics & Aeronautics*, Vol. 14, No. 4, April 1976.

[10] Gimmestad, D., "An Aeroelastic Optimization Procedure for Composite High Aspect Ratio Wings," Paper presented at the AIAA/ASME/ASCE/AHS 20th Structures, Structural Dynamics, and Materials Conference, St. Louis, Mo., April 1979.

[11] Gimmestad, D., "Aeroelastic Tailoring of a Composite Winglet for KC-135," Paper presented at AIAA/ASME/ASCE/AHS 22nd Structures, Structural Dynamics, and Materials Conference, Atlanta, Ga., April 1981.

[12] Triplett, W.E., "Aeroelastic Tailoring Studies in Fighter Aircraft," Paper presented at AIAA/ASME/ASCE/AHS 20th Structures, Structural Dynamics, and Materials Conference, St. Louis, Mo., April 1979.

[13] Rogers, W.A., Braymen, W.W., Murphy, A.C., Graham, D.H., and Love, M.H., "Validation of Aeroelastic Tailoring by Static Aeroelastic and Flutter Tests," AFWAL-TR-81-3160, Air Force Wright Aeronautical Laboratories, Wright-Patterson Air Force Base, Ohio, Sept. 1982.

[14] Lydick, L.N. and Mann, H.W., "Status Report on Development of a Variable Contour Wing Design for Fighter Aircraft," General Dynamics Report ERR-FW-1653, Dec. 1975.

[15] McCullers, L.A. and Naberhaus, J.D., "Automated Structural Design and Analysis of Advanced Composite Wing Models," *Computers and Structures*, Vol. 3, 1973, pp. 925-935.

[16] Brooks, J.D. and Beamish, J.K., "Measurements of Model Aeroelastic Deformations in the Wind Tunnel at Transonic Speeds Using Stereophotogrammetry," NASA Technical Paper 1010, 1977.

[17] Carmichael, R.L., Castellano, C.R., and Chen, F.C., "The Use of Finite Element Methods for Predicting the Aerodynamics of Wing-Body Combinations," NASA SP-228, Oct. 1969.

[18] Ballhaus, W.F., Bailey, F.R., and Frick, J., "Improved Computational Treatment of Transonic Flow About Swept Wings," *Advances in Engineering Science*, Vol. 4, NASA CP-2001, 1976, pp. 1311-1320.

[19] Bhateley, I.C., Mann, M.J., and Ballhaus, W.F., "Evaluation of Three-Dimensional Transonic Methods for the Analysis of Fighter Configurations," AIAA Paper 79-1528, July 1979.